applied optics

Low-loss reciprocal optical terminals for two-way time-frequency transfer

W. C. Swann,[1,*] L. C. Sinclair,[1] I. Khader,[1] H. Bergeron,[2] J.-D. Deschênes,[2] and N. R. Newbury[1]

[1]National Institute of Standards and Technology, 325 Broadway, Boulder, Colorado 80305, USA
[2]Université Laval, 2325 Rue de l'Université, Québec, Québec G1 V 0A6, Canada
*Corresponding author: william.swann@nist.gov

Received 18 August 2017; revised 29 September 2017; accepted 16 October 2017; posted 17 October 2017 (Doc. ID 305055); published 22 November 2017

We present the design and performance of a low-cost, reciprocal, compact free-space terminal employing tip/tilt pointing compensation that enables optical two-way time-frequency transfer over free-space links across the turbulent atmosphere. The insertion loss of the terminals is ~1.5 dB with total link losses of 15 dB, 24 dB, and 50 dB across horizontal, turbulent 2-km, 4-km, and 12-km links, respectively. The effects of turbulence on pointing control and aperture size, and their influence on the terminal design, are discussed.

OCIS codes: (120.0120) Instrumentation, measurement, and metrology; (120.3940) Metrology.

https://doi.org/10.1364/AO.56.009406

1. INTRODUCTION

Optical clock free-space networks could enable significant improvements in time distribution and precision navigation, contribute to the prospect of relativistic geodesy, as well as enable fundamental tests of physics [1–9]. To be successful, these networks need both precise optical clocks and high performance links between the clocks. Time/frequency transfer and clock comparisons have been successfully demonstrated in several fiber-based campaigns [1,4,7,10–15]. Free-space links can extend the range of clock networks to terrestrial locations where access to a fiber link is difficult, as well as to mobile and space-borne platforms. Combining fiber and free-space techniques could potentially result in a fully integrated time transfer system providing full global coverage. Indeed, programs such as the Time Transfer by Laser Link project [16] explore the prospect of free-space time transfer over global distances at the picosecond level. Other free-space time transfer efforts [17–23] explore transfer across a range of distances. A common thread through these efforts is the presence of atmospheric optical turbulence, which places constraints on the free-space optical (FSO) terminals at the link ends. These FSO terminals must be capable of supporting picosecond-to-femtosecond-level time-frequency transfer. Correction of turbulence-induced distortion of the received optical signal has been addressed in optical communications efforts using adaptive optics [24,25] as well as simpler tip/tilt control as used in [26]. In this paper, a pair of optical terminals optimized for frequency-comb-based optical two-way time-frequency transfer (O-TWTFT), using simple tip/tilt control, is presented.

Frequency-comb-based O-TWTFT [18,21–23] relies on the assumption that light will have the same time-of-flight as it travels in both directions between two transceivers, regardless of platform motion or turbulence. With this assumption, the difference in pulse arrival times at the two sites returns the clock offset between the sites independent of the time-of-flight variations for the pulse propagation. In O-TWTFT the measurement of this difference is achieved via a coherent two-way exchange of frequency comb pulses. We have explored O-TWTFT with several different measurement campaigns over optical links spanning between 2 and 12 km, shown in Fig. 1. We find the reciprocity in the time-of-flight, even over strongly turbulent air paths, is sufficient to allow frequency comparisons at the 10^{-19} level and synchronization at the sub-femtosecond level [21–23]. However, this level of time-frequency comparison is only possible if the transceivers, and particularly the FSO terminals, are designed to also maintain a high degree of reciprocity themselves. Indeed, the reciprocity requirements of O-TWTFT separate the design of the O-TWTFT FSO terminals from the myriad of free-space optical communications terminals designs presently in use. While the O-TWTFT terminals are compatible with high-speed free-space optical communications, the opposite is not true—all free-space optical communication terminals are not compatible with high-performance O-TWTFT, as it imposes additional requirements in terms of reciprocity and efficiency.

We emphasize that the reciprocity in the time-of-flight is true only for a single spatial mode and not for a multi-mode free-space link. Time-of-flight reciprocity is a consequence of the general reciprocity for a single spatial-mode propagation of light across a fixed turbulent atmosphere [27]. Atmospheric

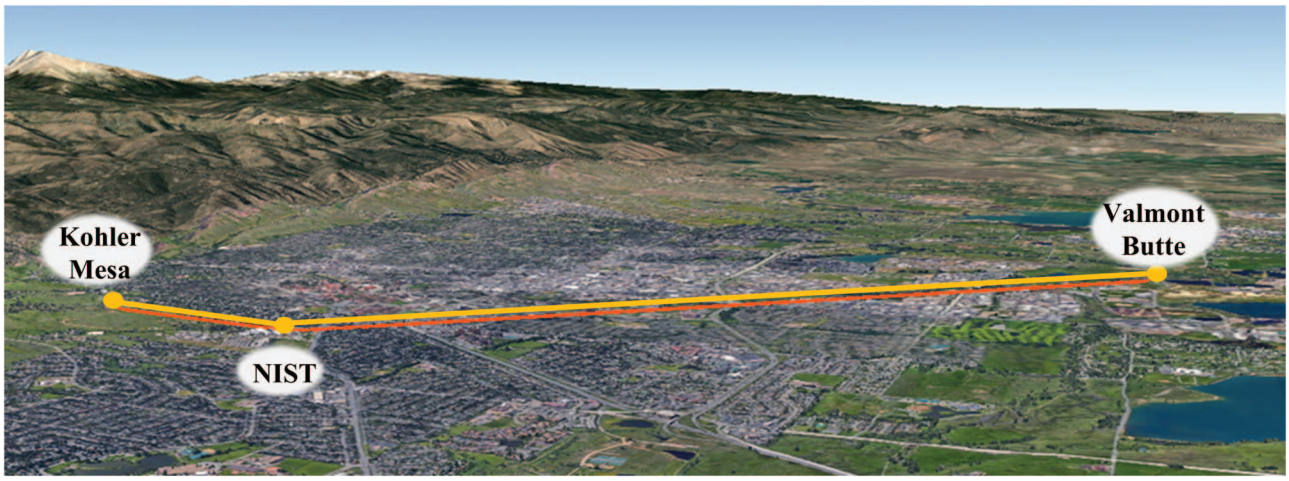

Fig. 1. Optical links over the city of Boulder. The launch/receive terminals reside in a rooftop laboratory at NIST, and the link intermediate points consist of remotely steered mirrors that return the signal to NIST. The Kohler Mesa path is 1-km long, for a 2-km round trip. This is doubled to 4 km via a second fold mirror in the rooftop laboratory. The Valmont Butte path is 6 km for a 12-km round trip. Image from Google Earth.

scintillation and fading also show reciprocal behavior [28,29], which can be exploited in free-space optical communication as well as providing convenient "markers" for coarse millisecond-level synchronization between sites for O-TWTFT. In addition, turbulence-induced beam pointing is identical for the received and transmitted modes at a given terminal; this is exploited, here as elsewhere, in a tip-tilt compensation for improved link availability by preferentially launching the transmitted power on the coupled mode. We first discuss the general requirements of FSO terminals for O-TWTFT, then the specific design of the terminals, and finally their performance. The design presented here is driven both by the fundamental requirements of O-TWTFT as well as practical considerations, such as cost, robustness, and size. The terminals are predominately constructed from commercial off-the-shelf components while simple custom-machined component mounts contribute to compactness and ruggedness of the design; as presented they are constructed at a cost of approximately US$12,000 per terminal at the time of publication. This costing includes all terminal optics, and the tip/tilt mirror control electronics, but excludes the gimbal, and the frequency comb and beacon lasers. As optical networks expand beyond simple demonstrations of point-to-point links, the practical considerations will take on a greater importance as each optical network node will require at least one free-space optical terminal if not more, depending on the network topology. Furthermore, the simple design and low cost of the terminals, combined with the decreasing cost of frequency comb sources, should expand the exploration of O-TWTFT and other transfer techniques.

2. BASIC REQUIREMENTS

A. Terminal Reciprocity

As stated, O-TWTFT can support femtosecond (fs)-level performance only if the measurement path is single-mode over its entire length, including through the terminals. This places several demands on the terminal design. First, as is obvious from above, multi-mode fiber cannot be used to couple signals into and out of the terminals. Second, in preserving reciprocity, the terminals must be bi-directional, meaning they must avoid the use of circulators or other non-reciprocal fiber-optic devices that separate the outgoing and return paths. Third, they should be fully polarization-maintaining (including the single-mode fiber), thus avoiding birefringence that can lead to non-reciprocal time-of-flight.

Fortunately, this choice of single-mode polarization-maintaining fiber is not only compatible but also required by the heterodyne signal detection used in O-TWTFT. Direct detection, as is used in many free-space optical communication systems, cannot support the fs-level timing precision available from state-of-the-art optical clocks. Instead, the timing signals are provided by optical frequency combs, locked to their respective local clocks, and detection is performed through linear optical sampling (heterodyne detection) of the received signal against the local comb [18,21].

B. Terminal Insertion Loss

In addition to reciprocity, the FSO terminals must support efficient detection of the frequency comb pulses. Our present detection requires ~100 photons per pulse. At our 200-MHz comb repetition rate, this corresponds to an average power of 2.5 nW. With additional signal processing (to reject noise or ghost signals), the detection limit might drop to ~10 photons per pulse. Because of atmospheric scintillation, the actual received power will fluctuate strongly across a single-mode link and the required power level then acts as a threshold. Received power below this threshold results in a "fade" where no timing information is retrieved. In contrast to most optical communications systems where such fades require data buffering and retransmission, O-TWTFT can easily ride over such fades [22]. Nevertheless, for the highest performance, one would like the most power margin—i.e., the maximum received power, which leads to additional constraints on the terminal design.

Clearly, to maximize the power margin, the insertion loss of the terminals due to reflections, absorption, or occlusions

should be minimized. This requirement is also true in free-space communications, but in that case loss is more easily compensated by use of an erbium-doped fiber amplifier. Penalty-free amplification of the comb pulse train in O-TWTFT is more problematic. Bi-directional amplification can preserve reciprocity but an amplifier designed for maximum power of the outgoing comb light will not perform well as a low-noise signal amplifier for the weak incoming comb light (and vice versa). Use of separate amplifiers for outgoing and incoming signals leads to a breakdown in reciprocity, requiring exacting compensation of the separate amplifier path lengths to maintain femtosecond timing. To further constrain the power requirements, the emitted light may be limited to the "eye-safe" regime of 100 mW/cm^2, especially for ground-level horizontal links.

Here, we take the approach of designing the terminals for low insertion loss. Our terminals have an insertion loss of only ~1.5 dB, making maximum use of the available comb power. This avoids the need for amplification of the ~5-mW comb light for link distances of up to 12 km, although longer distances will require incorporation of power amplifiers for the outgoing signal. For optimum performance, these low-loss terminals must nevertheless incorporate correction for atmospheric pointing by (at a minimum) angular tip/tilt control of the beams to compensate for turbulence, which leads to the use of a separate beacon laser, as discussed later.

C. Compensation for Atmospheric Turbulence

Atmospheric turbulence perturbs both the amplitude and phase of the beam projected between two FSO terminals. The zeroth-order phase perturbation, i.e., the "piston" noise, which appears as a timing delay, is identically compensated for by the two-way transfer and is invisible to the coupling of light through the terminals. The first-order phase perturbation, the angle-of-arrival noise, significantly impacts the beam coupling through the terminal and into the single-mode fiber, and as such needs active compensation. For typical turbulence conditions over near-ground optical links, the atmospheric refractive index structure constant C_n^2 varies from ~10^{-13} to 10^{-16} m$^{-2/3}$, with a typical value of 10^{-14} m$^{-2/3}$ near the ground in Boulder, Colorado [30,31]. This translates to an angle of arrival jitter α on the received beam given by $\alpha \sim 2.9L\ C_n^2/D^{1/3}$, where D is the terminal's aperture diameter, L is the path length, and C_n^2 is assumed uniform over the path [32]. Over a ~12-km link and our aperture diameter of 48 mm, this translates to α varying between 3 and 100 μrad. The jitter frequency spectrum cuts off sharply at frequencies above $V/2\pi D$, where V is the wind speed; for $V < 10$ m/s the jitter remains primarily below 340 Hz [32]. The upper limits in these values in turn set a lower limit on the performance of the terminal's angle of arrival compensation control, which is implemented using a quadrant detector and tip/tilt mirror, as discussed below. Removing the received signal's angle of arrival jitter also pre-compensates the angle of the emitted light, in effect establishing the single-mode reciprocity of the entire link.

In addition to angle of arrival jitter, turbulence adds an overall "waviness" to the received phase fronts, which in turn defines the terminal's aperture size. The extent over which a phase front varies by less than ~1 rad is referred to as the coherence size or Fried parameter r_0 [33], and sets an upper limit on the size of the collection aperture for which received light can be efficiently coupled into a single-mode fiber (or used directly for heterodyne detection). Figure 2 shows r_0 for both horizontal paths and slant paths, as would be used between a ground station and an aerial platform [30]. Based on these plots, in constructing the FSO terminals, an aperture size of 48 mm is chosen, allowing efficient collection over 2- to 20-km paths having a path averaged C_n^2 between 10^{-14} and 10^{-15} m$^{-2/3}$. Choosing a 48-mm aperture also allows for a wide selection of off-the-shelf commercial optics. Adaptive optics (AO) can in principle be used to increase the aperture size by compensating for higher-order turbulence effects [30,34] and in fact have been used in free-space optical communications settings [24,25,35,36] as well as for time transfer [23,37]. However, such systems require that a significant amount of the signal power be used for the AO phase front sensor. Furthermore, AO systems tend to be expensive and complex.

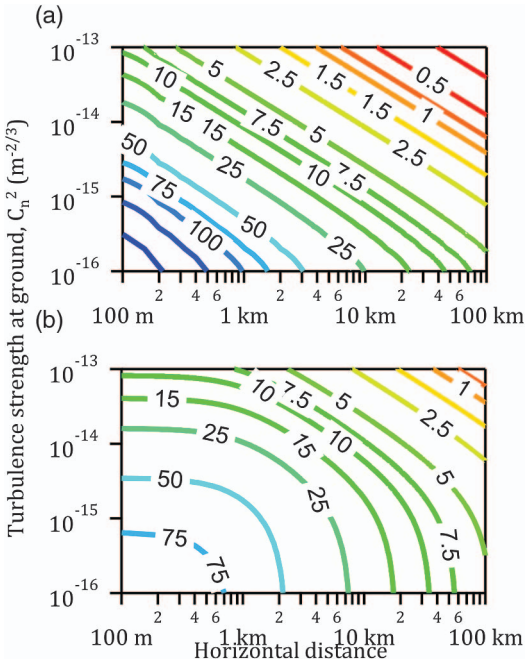

Fig. 2. Contour plot of the Fried parameter (maximum useful aperture diameter) in centimeters for a single-mode optical link as a function of turbulence strength, measured on the ground, and the horizontal distance along the ground. The path itself is assumed to be either (a) along the ground or (b) to slant vertically upward to an Aerial (or mountaintop) platform at 1-km elevation. These calculations assume a standard Hufnagel-Valley profile [17] and an upper atmosphere wind speed of 21 m/s.

3. FREE-SPACE OPTICAL TERMINAL DESIGN

A. Optical Layout

The bi-directional FSO terminal design is shown in Fig. 3, and is loosely based on the design presented in [38]. The transmitted frequency comb signal light enters the terminal via a polarization-maintaining single-mode fiber, where it is collimated into a ~3-mm diameter beam, directed to a

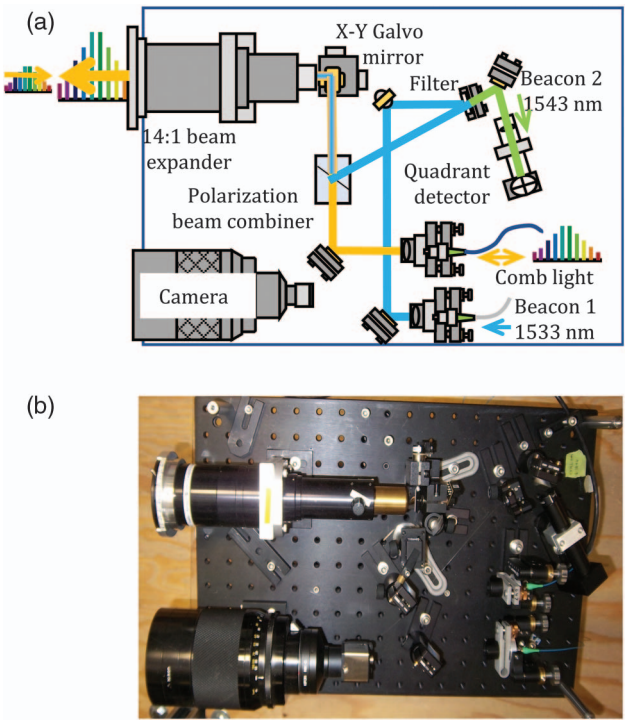

Fig. 3. FSO terminal (a) design and (b) photo. The signal (comb light) path is fully bi-directional; the transmitted and received comb signals pass through the same fiber entering the terminal. The beacons are bi-directional (and co-collimated with the signal) up to the filter, where the received beacon is separated and directed onto a quadrant detector. The quadrant detector signal acts on the galvo mirror to center the received beacon onto the detector. The received comb signal is then efficiently passively coupled into its fiber.

commercially available tip/tilt galvo mirror, and then to a 14∶1 Keplerian beam expander (defined by having a positive focus secondary lens) with a 48-mm aperture. The Keplerian design is chosen so that the secondary lens conjugate point lies outside the expander; placing the galvo mirror at this point eliminates the conversion of tip/tilt to displacement jitter. Should cost-effective AO systems of sufficient performance in the 1550-nm band become available, the AO system's deformable mirror would be placed at this location. The Gaussian primary beam exiting the expander aperture has a $1/e^2$ intensity radius of 20 mm. The narrow wavelength range over which the system operates (~1530–1570 nm) allows for use of refractive optics, negating problems associated with reflective optics including alignment complications with off-axis parabolic mirrors and signal loss due to the central occlusion of Cassegrain-type receivers common in optical communications systems. As a receiver, the terminal acts "in reverse"; light entering the aperture is directed off the galvo mirror and to the fiber, which itself is bi-directional, acting to both transmit and receive the timing signals.

With this simple design, the insertion loss for the signal light is only 1.5 dB per terminal, given by the transmission through the optics and coupling into the fiber. The theoretical Strehl ratio is 0.8, as defined by the aperture radius, $r_A = 24$ mm, backpropagated to the fiber core and overlapped with the fiber mode [39]. This, of course, drops with turbulence and a corresponding decrease in the Fried parameter, and the Strehl ratio is measured to be between 0.3 and 0.6 depending on the turbulence strength. To explore link behavior versus aperture size in the face of varying coherence size, the terminal apertures are fitted with irises that can be varied in size from a few millimeters to the full aperture of 48 mm. (It is noted that the terminal's nominal 5-cm [2-in.] commercially available lenses have their aperture reduced to 48 mm by the lens mounting hardware.)

A separate beacon laser, which provides the error signal for the tip/tilt control, is similarly collimated into a 3-mm diameter beam and polarization-multiplexed with the signal beam through a Glan-laser polarization combiner. This beacon beam is carefully co-aligned and co-collimated with the signal beam so that the two beams sample the same atmospheric mode volume across the link. To prevent cross talk, the beacons at each terminal have wavelengths distinct from each other and from the signal light. Our system uses beacons at 1532 nm and 1542 nm, and the signal comb light lies in a ~10-nm band between 1550 and 1560 nm. The small separation between these wavelengths is not expected to have any effect on the system performance, based on the following argument. The coherence size r_0 is given, for example, by Eq. 38 in [32]; taking the derivative of this with respect to $k(=2\pi/\lambda)$ and solving for $\Delta\lambda \sim 25$ nm between the comb signal and beacons, reveals a change in r_0 of <2% across this wavelength span. This small difference is not expected to have any differential effect on the coupling of the beacon versus the comb signal into the terminal. Angle of arrival jitter and other turbulence-driven effects are expected to scale similarly. However, these wavelengths are far enough apart to be easily separated with narrowband filters. The received beacon is de-multiplexed from the signal, passes through a narrowband interference filter, and is focused through a lens onto a quadrant detector. This focusing lens is necessary so that the detection is sensitive only to angle of arrival jitter and insensitive to lateral offsets. By using a telephoto design, this lens provides a relatively large ~100-μm focused spot on the 3-mm diameter detector surface, giving the quadrant detection reasonable linearity. In setting up the terminals, the received beacon is adjusted so that it is centered on the quadrant detector commensurate with the received signal being centered on its fiber.

B. Feedback Control

A digital feedback loop keeps the received beacon centered on the quadrant detector by controlling the tip-tilt galvo mirror. The control system comprises an inexpensive, commercially available field-programmable gate array controller running a proportional-integral loop for each of the X and Y quadrant detector error signals. The loop halts operation when the signal fades, preventing the galvo from railing, and restores operation when the signal returns. Configuration settings, as well as displays of received beacon power, error signal, and control effort, are all displayed on a PC interface. The system performs well with only integral gain. The servo bandwidth is limited to ~1.2 kHz by the galvo mirror, above the bandwidth necessary for angle of arrival jitter compensation but below the bandwidth of the controller.

The terminals are mounted on a pair of gimbals for coarse pointing and occasional alignment optimization. The galvo mirrors provide enough dynamic range to compensate for milliradian-scale pointing drifts. However, the gimbals do require occasional manual alignment (which can be done while measurements were running) for continuous days-long measurement runs, although this function could be included in the feedback loop as a high dynamic range, slow response outer loop. Presently, initial acquisition between the link ends is established using a visible-wavelength camera having a 500-mm focal length lens co-aligned with the terminal optics. The same camera image with image recognition software, along with a second, visible wavelength beacon, could be used for acquisition and gimbal tracking under demanding dynamic situations, as is done in [40].

4. PERFORMANCE OF FREE-SPACE OPTICAL TERMINALS

A. Measurement Paths and Return Power

The FSO terminals were used in several measurement campaigns demonstrating O-TWTFT over horizontal paths of 2–12 km. Typical launched signal power is between 3 and 5 mW. The received power is at or below ~8 μW, depending on path length and turbulence, and shows significant effects of turbulence-induced scintillation, often dropping to zero for short durations, as seen in Fig. 4(c) for the 4-km path. In all cases a folded beam path geometry is used, consisting of a fold mirror at the intermediate point of the path [see Figs. 1 and 4(a)]. This places the terminals next to one another, enabling out-of-loop "truth" measurements of the time transfer across the link [21–23]. The doubly folded 4-km Kohler Mesa link, also shown in Fig. 1, has two 50-cm diameter mirrors, which allows switching between 2 and 4 km. The height above ground varies smoothly between 15 m and 30 m over most of this link. The 12-km link to Valmont Butte has a single 40-cm diameter remote mirror; the height above ground varies between 30 and 45 m over most of this link. The mirrors for both links reside on tops of steep inclines, and the rooftop laboratory from which both links emanate is at a height of roughly 15 m. Atmospheric turbulence is monitored by an independent scintillometer which returned a value for C_n^2. However, in some cases the received power is significantly less than predicted by the ratio r_0/r_s, where r_s is the turbulence-induced beam spread derived from the scintillometer reading [32]. The disagreement is likely associated with an underrepresentation of C_n^2, as the scintillometer does not account for turbulence concentrated at the path ends, as might be driven by solar heating of the structures housing the terminals and mirror, or the air exchange across the laboratory window openings through which the signals are launched and received. In other cases, the received power agrees with that predicted by using the value of r_s derived from the scintillometer reading, indicating uniform turbulence along the path.

The effect of turbulence becomes obvious by examining the structure of the received signal light. Figure 4(b) shows images,

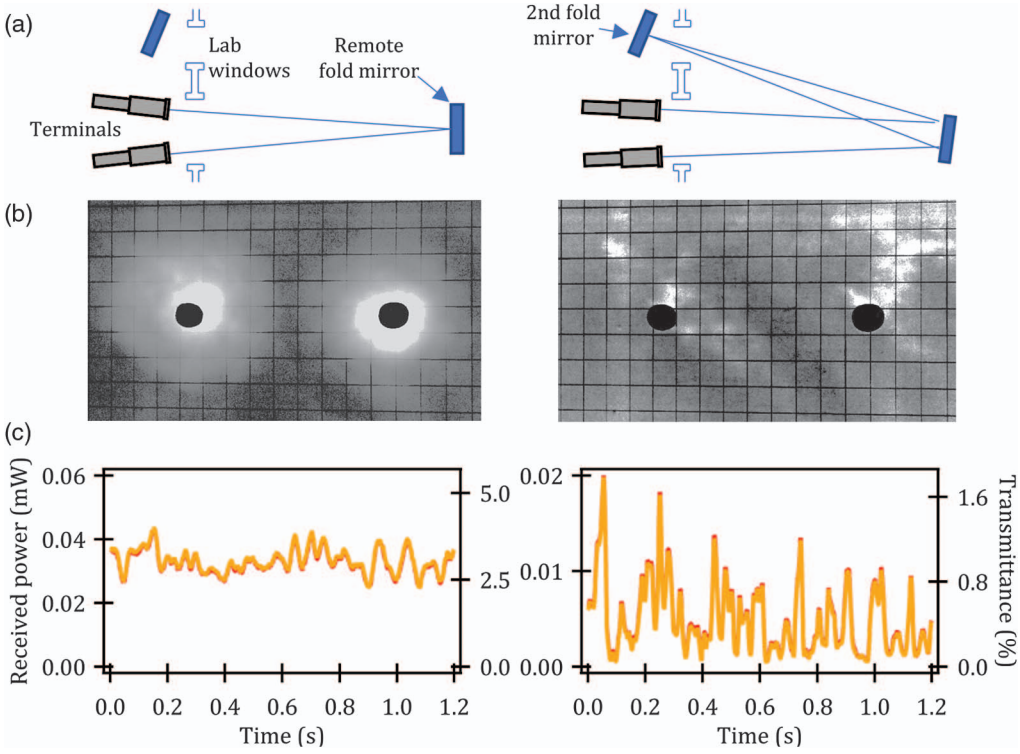

Fig. 4. Left panel: results for a 2-km link to Kohler mesa under low turbulence. Right panel: results for a 4-km link to Kohler mesa under moderate turbulence. (a) Folded link geometry (see also Fig. 1). (b) Received beam spot viewed directly in front of the terminals, on a 5-cm grid. The dark circles are holes through which the beams exit and enter the terminals. (c) Received power (left axis) and percentage link transmittance (right axis) versus time. Received power in both terminals is shown in red and orange, though the traces lie on top of one another, as expected for a single-mode link because of reciprocity.

on a 5-cm grid, of the received beams for the 2- and 4-km paths, under low and moderate turbulence, respectively. The 2-km path shows a single, concentrated spot centered on the receive terminal whereas the 4-km path shows significant scintillation. Figure 4(c) shows the received signal power and link transmittance for a launched power of 1.16 mW. For the low turbulence 2-km link, the average received power is 0.033 mW, giving a link transmittance of 2.8%. For the moderate turbulence 4-km link the average received power and transmittance are 0.0043 mW and 0.37%, respectively.

B. Signal and Beacon Co-Collimation

A measurement campaign to synchronize clocks over a 12-km horizontal path [23] dramatically illustrates the need for proper co-collimation of the beacon and signal light in the presence of strong path-averaged turbulence strengths. Figure 5 shows the effect of a divergent versus co-collimated beacon, where a remarkable ~10-fold increase in received power and sixfold reduction in timing jitter are seen by co-collimating the signal and beacon beams. We explain this behavior as follows. With a divergent beacon and collimated signal beam, the beacon and signal beams sample different atmospheric turbulence volumes. As such, the resulting turbulence-induced phase perturbations, which include the angle of arrival, for the signal and beacon beams entering a terminal are uncorrelated. The feedback corrects for the angle of arrival of the beacon, which may not properly correct for the signal's angle of arrival. This lack of correlation between the (corrected) beacon and the signal results in a signal that only randomly couples into the signal fiber, leading to lower average coupled power and a higher rate of fades, in turn resulting in higher timing noise, as seen in Fig. 5(a). This is different from the situation in sub-kilometer-scale optical communications links where the integrated turbulence is not strong enough to reduce the Fried parameter to the beam diameters. Here, divergent beacon beams are used quite successfully, even for heterodyne detection configurations [38], as well as in situations where multi-mode direct detection is used.

C. Beacon Correlation Versus Aperture Size

As mentioned earlier, at high turbulence, the signal comb light effectively sees a receive aperture set by the Fried parameter r_0 that is smaller than the physical aperture sampled by the beacon laser. To explore this behavior, we can stop down the receive aperture via an iris. Figure 6 shows received beacon and signal intensities versus aperture iris size over the 4-km link. In Fig. 6(a), the aperture is open fully to 48 mm and poor correlation is seen between the two beacons and the signal. C_n^2 is estimated to be $\sim 1.5 \times 10^{-14}$ for these data, giving a Fried coherence size r_0 of ~22 mm; only signal light covering a region of this size couples into the signal fiber. On the other hand, all the beacon light entering the terminal couples to the quadrant detector, leading to the lack of correlation between the signal and beacons in Fig. 6(a). As the aperture is reduced to roughly r_0 [Fig. 6(b)] only a single coherence region enters the terminal. The feedback centers the beacon onto the quadrant detector, and because the signal and beacon occupy the same mode, and due to the *a priori* alignment of the quadrant detector and signal collimator axes, the signal comb light is centered on the fiber core. Full reciprocity for both the beacons and signals is now established, as seen in the high degree of correlation between the signals and beacons in Fig. 6(b). Note that in both cases the signal itself is correlated at the two link ends; this is a consequence of the fundamental reciprocity of the single-mode coupling between the single-mode signal fibers at the two link ends, which is independent of the beacons.

This behavior has important implications in the single-mode detection of the signal. With the aperture matched to (or smaller than) r_0, single-mode behavior is expected. In strong turbulence, when r_0 is significantly smaller than the aperture the situation is more complicated. The fiber coupling is still single mode; however, the frequency and duration over which the signal couples into the fiber becomes more random, due to the multi-mode nature of the beacons. One might expect an increase in performance as the aperture is reduced to r_0; however, reduction in aperture size will also decrease the detected power because the launched beam is clipped by the aperture,

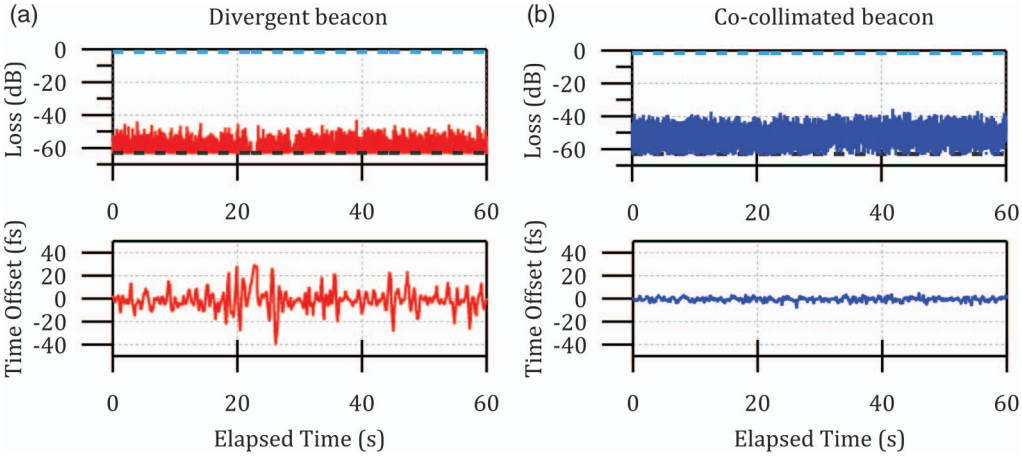

Fig. 5. Results at 12 km for a beacon beam which is (a) co-aligned but differentially divergent from the signal light and (b) co-aligned and co-collimated with the signal light. The launched signal power is 3.5 mW and the turbulence strength is $C_n^2 \sim 10^{-14}$ $m^{-2/3}$. For a co-collimated beacon as opposed to a divergent beacon, the link loss is reduced by a factor of 10 and the out-of-loop time offset correspondingly improves from 50 fs peak-to-peak to 8 fs peak-to-peak.

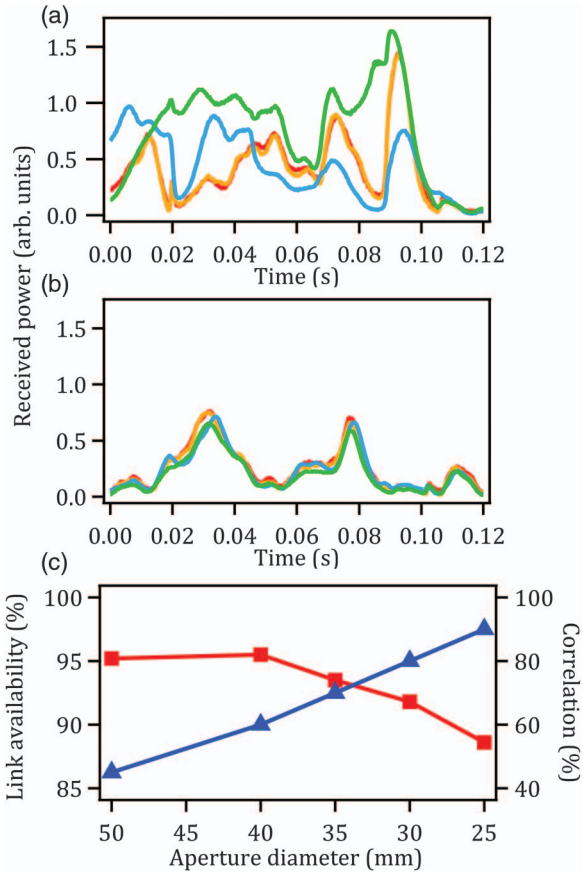

Fig. 6. Received signal power (red, orange) and beacon power (blue, green) into the left and right terminals, respectively, for an aperture of (a) 48-mm diameter and (b) 25-mm diameter. For these data at 4-km link and $C_n^2 = 1.5 \times 10^{-14}$ $m^{-2/3}$, the Fried parameter is 22 mm, leading to the high correlation observed for the 25-mm diameter aperture. (c) The link availability (red squares) and correlation between the signal and beacon light (blue triangles) versus aperture diameter.

directly reducing its power as well as increasing its divergence. This behavior is seen in Fig. 6(c), which displays both the correlation between the beacons at the link ends and the "link availability" (which is essentially a measure of the time the received signal power is above detection threshold) versus aperture size. These measurements were made at lower turbulence than those of Figs. 6(a) and 6(b). As the aperture is decreased from fully open to 40 mm, negligible change in the link availability is seen, but the correlation between the link ends increases from 45% to 60%. As the aperture is reduced further the correlation continues to increase but the received power drops. The overall decrease in signal strength as the aperture iris is closed is a consequence of the clipping of the transmitted signal beam by the iris; this suggests a more evolved terminal design where the beam expander itself can be "zoomed" to where the output beam diameter is matched to r_0, thus preserving launch power. However, the increased complexity of such a design is outside the scope of this work. Another approach to increasing efficiency is to have several single-mode receivers within a terminal having a larger aperture, as described in [41], or have multiple apertures, as in [28].

5. CONCLUSIONS

The free-space optical terminal design presented here supports fs-level O-TWTFT with operation demonstrated over horizontal air paths up to 12 km in length. The low-loss optical design of these terminals allows for operation over horizontal, near-ground paths under moderate-to-severe turbulence conditions while emitting power at eye-safe levels at 1550 nm. They are robust enough to allow for field operation, and are small and light enough to be considered for airborne operation. This design can support future efforts to perform time-transfer measurements in a network configuration for which pairs of terminals will be required at each node of the network. For instance, this geometry could support long indirect links over slant paths to an aerial platform repeater, where the lower turbulence at higher altitudes reduces scintillation. From Fig. 2, slant paths of ~100 km should be achievable. Furthermore, operation of the terminals in an environment where eye safety concerns can be relaxed allows for the possible addition of amplification, at some cost in reciprocity. Finally, the use of low-loss terminals in a network configuration allows for ring and other path geometries that could be used in tests of geodesy or special relativity.

Funding. DARPA Defense Sciences Office (DSO) PULSE program; National Institute of Standards and Technology (NIST).

Acknowledgment. We thank Esther Baumann, Ian Coddington, Kevin Cossel, and Tasshi Dennis for helpful comments.

REFERENCES

1. F. Riehle, "Optical clock networks," Nat. Photonics **11**, 25–31 (2017).
2. T. Takano, M. Takamoto, I. Ushijima, N. Ohmae, T. Akatsuka, A. Yamaguchi, Y. Kuroishi, H. Munekane, B. Miyahara, and H. Katori, "Geopotential measurements with synchronously linked optical lattice clocks," Nat. Photonics **10**, 662–666 (2016).
3. A. Derevianko and M. Pospelov, "Hunting for topological dark matter with atomic clocks," Nat. Phys. **10**, 933–936 (2014).
4. C. Lisdat, G. Grosche, N. Quintin, C. Shi, S. M. F. Raupach, C. Grebing, D. Nicolodi, F. Stefani, A. Al-Masoudi, S. Dörscher, S. Häfner, J.-L. Robyr, N. Chiodo, S. Bilicki, E. Bookjans, A. Koczwara, S. Koke, A. Kuhl, F. Wiotte, F. Meynadier, E. Camisard, M. Abgrall, M. Lours, T. Legero, H. Schnatz, U. Sterr, H. Denker, C. Chardonnet, Y. Le Coq, G. Santarelli, A. Amy-Klein, R. Le Targat, J. Lodewyck, O. Lopez, and P.-E. Pottie, "A clock network for geodesy and fundamental science," Nat. Commun. **7**, 12443 (2016).
5. C. Guerlin, P. Delva, and P. Wolf, "Some fundamental physics experiments using atomic clocks and sensors," C. R. Phys. **16**, 565–575 (2015).
6. C. W. Chou, D. B. Hume, T. Rosenband, and D. J. Wineland, "Optical clocks and relativity," Science **329**, 1630–1633 (2010).
7. P. Delva, J. Lodewyck, S. Bilicki, E. Bookjans, G. Vallet, R. Le Targat, P.-E. Pottie, C. Guerlin, F. Meynadier, C. Le Poncin-Lafitte, O. Lopez, A. Amy-Klein, W.-K. Lee, N. Quintin, C. Lisdat, A. Al-Masoudi, S. Dörscher, C. Grebing, G. Grosche, A. Kuhl, S. Raupach, U. Sterr, I. R. Hill, R. Hobson, W. Bowden, J. Kronjäger, G. Marra, A. Rolland, F. N. Baynes, H. S. Margolis, and P. Gill, "Test of special relativity using a fiber network of optical clocks," Phys. Rev. Lett. **118**, 221102 (2017).
8. R. Bondarescu, M. Bondarescu, G. Hetényi, L. Boschi, P. Jetzer, and J. Balakrishna, "Geophysical applicability of atomic clocks: direct continental geoid mapping," Geophys. J. Int. **191**, 78–82 (2012).

9. B. Altschul, Q. G. Bailey, L. Blanchet, K. Bongs, P. Bouyer, L. Cacciapuoti, S. Capozziello, N. Gaaloul, D. Giulini, J. Hartwig, L. Iess, P. Jetzer, A. Landragin, E. Rasel, S. Reynaud, S. Schiller, C. Schubert, F. Sorrentino, U. Sterr, J. D. Tasson, G. M. Tino, P. Tuckey, and P. Wolf, "Quantum tests of the Einstein equivalence principle with the STE-QUEST space mission," Adv. Space Res. **55**, 501–524 (2015).
10. S. Droste, F. Ozimek, T. Udem, K. Predehl, T. W. Hänsch, H. Schnatz, G. Grosche, and R. Holzwarth, "Optical-frequency transfer over a single-span 1840 km fiber link," Phys. Rev. Lett. **111**, 110801 (2013).
11. C. E. Calosso, E. Bertacco, D. Calonico, C. Clivati, G. A. Costanzo, M. Frittelli, F. Levi, A. Mura, and A. Godone, "Frequency transfer via a two-way optical phase comparison on a multiplexed fiber network," Opt. Lett. **39**, 1177–1180 (2014).
12. Z. Jiang, A. Czubla, J. Nawrocki, W. Lewandowski, and E. F. Arias, "Comparing a GPS time link calibration with an optical fibre self-calibration with 200 ps accuracy," Metrologia **52**, 384–391 (2015).
13. M. Xin, K. Şafak, M. Y. Peng, A. Kalaydzhyan, W.-T. Wang, O. D. Mücke, and F. X. Kärtner, "Attosecond precision multi-kilometer laser-microwave network," Light Sci. Appl. **6**, e16187 (2017).
14. W.-K. Lee, F. Stefani, A. Bercy, O. Lopez, A. Amy-Klein, and P.-E. Pottie, "Hybrid fiber links for accurate optical frequency comparisons," arXiv: 170201687 (2017).
15. A. Bercy, F. Stefani, O. Lopez, C. Chardonnet, P.-E. Pottie, and A. Amy-Klein, "Two-way optical frequency comparisons at 5×10^{-21} relative stability over 100-km telecommunication network fibers," Phys. Rev. A **90**, 061802 (2014).
16. E. Samain, P. Exertier, P. Guillemot, P. Laurent, F. Pierron, D. Rovera, J. Torre, M. Abgrall, J. Achkar, D. Albanese, C. Courde, K. Djeroud, M. L. Bourez, S. Leon, H. Mariey, G. Martinot-Lagarde, J. L. Oneto, J. Paris, M. Pierron, and H. Viot, "Time transfer by laser link—T2L2: current status and future experiments," in *Joint Conference of the IEEE International Frequency Control and the European Frequency and Time Forum (FCS)* (2011), pp. 1–6.
17. K. Djerroud, E. Samain, A. Clairon, O. Acef, N. Man, P. Lemonde, and P. Wolf, "A coherent free space optical link for long distance clock comparison, navigation, and communication: the mini-doll project," in *International Conference on Space Optics* (2010).
18. F. R. Giorgetta, W. C. Swann, L. C. Sinclair, E. Baumann, I. Coddington, and N. R. Newbury, "Optical two-way time and frequency transfer over free space," Nat. Photonics **7**, 434–438 (2013).
19. J. Conklin, N. Barnwell, L. Caro, M. Carrascilla, O. Formoso, S. Nydam, P. Serra, and N. Fitz-Coy, "Optical time transfer for future disaggregated small satellite navigation systems," in *AIAAUSU Conference on Small Satellites* (2014).
20. J. Kang, J. Shin, C. Kim, K. Jung, S. Park, and J. Kim, "Few-femtosecond-resolution characterization and suppression of excess timing jitter and drift in indoor atmospheric frequency comb transfer," Opt. Express **22**, 26023–26031 (2014).
21. J.-D. Deschênes, L. C. Sinclair, F. R. Giorgetta, W. C. Swann, E. Baumann, H. Bergeron, M. Cermak, I. Coddington, and N. R. Newbury, "Synchronization of distant optical clocks at the femtosecond level," Phys. Rev. X **6**, 021016 (2016).
22. H. Bergeron, L. C. Sinclair, W. C. Swann, C. W. Nelson, J.-D. Deschênes, E. Baumann, F. R. Giorgetta, I. Coddington, and N. R. Newbury, "Tight real-time synchronization of a microwave clock to an optical clock across a turbulent air path," Optica **3**, 441–447 (2016).
23. L. C. Sinclair, W. C. Swann, H. Bergeron, E. Baumann, M. Cermak, I. Coddington, J.-D. Deschênes, F. R. Giorgetta, J. C. Juarez, I. Khader, K. G. Petrillo, K. T. Souza, M. L. Dennis, and N. R. Newbury, "Synchronization of clocks through 12 km of strongly turbulent air over a city," Appl. Phys. Lett. **109**, 151104 (2016).
24. Z. Sodnik, J. P. Armengol, R. H. Czichy, and R. Meyer, "Adaptive optics and ESA's optical ground station," Proc. SPIE **7464**, 746406 (2009).
25. M. W. Wright, J. F. Morris, J. M. Kovalik, K. S. Andrews, M. J. Abrahamson, and A. Biswas, "Adaptive optics correction into single mode fiber for a low Earth orbiting space to ground optical communication link using the OPALS downlink," Opt. Express **23**, 33705–33712 (2015).
26. H. Takenaka, M. Toyoshima, and Y. Takayama, "Experimental verification of fiber-coupling efficiency for satellite-to-ground atmospheric laser downlinks," Opt. Express **20**, 15301–15308 (2012).
27. J. H. Shapiro, "Reciprocity of the turbulent atmosphere," J. Opt. Soc. Am. **61**, 492–495 (1971).
28. R. R. Parenti, J. M. Roth, J. H. Shapiro, F. G. Walther, and J. A. Greco, "Experimental observations of channel reciprocity in single-mode free-space optical links," Opt. Express **20**, 21635–21644 (2012).
29. D. Giggenbach, W. Cowley, K. Grant, and N. Perlot, "Experimental verification of the limits of optical channel intensity reciprocity," Appl. Opt. **51**, 3145–3152 (2012).
30. L. C. Andrews and R. L. Phillips, *Laser Beam Propagation through Random Media*, 2nd ed. (SPIE, 2005).
31. D. K. Killinger, J. H. Churnside, and L. S. Rothman, "Atmospheric optics," in *OSA Handbook of Optics* (McGraw-Hill, 2004), Vol. **4**.
32. R. L. Fante, "Electromagnetic beam propagation in turbulent media," Proc. IEEE **63**, 1669–1692 (1975).
33. D. L. Fried, "Optical heterodyne detection of an atmospherically distorted signal wave front," Proc. IEEE **55**, 57–77 (1967).
34. F. Roddier, "The effects of atmospheric turbulence in optical astronomy," in *Progress in Optics*, E. Wolf, ed. (North-Holland, 1981), Vol. **19**, pp. 281–376.
35. L. B. Stotts, B. Stadler, D. Hughes, P. Kolodzy, A. Pike, D. W. Young, J. Sluz, J. Juarez, B. Graves, D. Dougherty, J. Douglass, and T. Martin, "Optical communications in atmospheric turbulence," Proc. SPIE **7464**, 746403 (2009).
36. J. C. Juarez, D. W. Young, R. A. Venkat, D. M. Brown, A. M. Brown, R. L. Oberc, J. E. Sluz, H. A. Pike, and L. B. Stotts, "Analysis of link performance for the FOENEX laser communications system," Proc. SPIE **8380**, 838007 (2012).
37. K. Petrillo, M. L. Dennis, J. C. Juarez, E. Baumann, H. Bergeron, I. Coddington, J.-D. Deschênes, F. R. Giorgetta, N. R. Newbury, and W. C. Swann, "Enhanced link availability for FSO time-frequency transfer using adaptive optic terminals," in *Atmospheric Propagation XIII* (2016), pp. 9833–9838.
38. Y. Arimoto, "Compact free-space optical terminal for multi-gigabit signal transmissions with a single-mode fiber," Proc. SPIE **7199**, 719908 (2009).
39. P. J. Winzer and W. R. Leeb, "Fiber coupling efficiency for random light and its applications to lidar," Opt. Lett. **23**, 986–988 (1998).
40. K. C. Cossel, E. M. Waxman, F. R. Giorgetta, M. Cermak, I. R. Coddington, D. Hesselius, S. Ruben, W. C. Swann, G.-W. Truong, G. B. Rieker, and N. R. Newbury, "Open-path dual-comb spectroscopy to an airborne retroreflector," Optica **4**, 724–728 (2017).
41. Y. Dikmelik and F. M. Davidson, "Fiber-coupling efficiency for free-space optical communication through atmospheric turbulence," Appl. Opt. **44**, 4946–4952 (2005).